International Journal of Marine Engineering Innovation and Research, Vol. 11(3), Sept. 2026. 1005-1013
(pISSN: 2541-5972, eISSN: 2548-1479)

Environmental-Oriented Enhancement of B40 Biodiesel Combustion Efficiency Using Hybrid PtO_2–CeO_2 Catalyst and Neodymium N45 Magnetic System in Diesel Engines

Sutrisno[1*], Hadi Prasutiyon[2], Erik Sugianto[3], Muchlas Adi Sunjaya[4]

(Received: 12 May 2026 / Revised: 16 May 2026 / Accepted: 25 May 2026 / Available Online: 1 September 2026)

***Abstract*—** The mandatory B40 biodiesel policy in Indonesia has introduced significant technical challenges for diesel engine operation, including increased fuel viscosity, reduced atomization quality, and elevated specific fuel consumption (SFC). This study presents the design, CFD simulation, and experimental validation of a novel hybrid fuel treatment device combining 20 pieces of bipolar neodymium N45 permanent magnets (magnetization zone, peak field 2800 Gauss) with a packed-bed of 6 PtO_2–CeO_2 bimetallic donut-shaped (toroid) catalysts (catalytic zone). CFD simulations using ANSYS Fluent 2024 R1 were conducted to characterize the magnetic field distribution, velocity profile, pressure drop (ΔP = 2.30 bar), catalytic reaction rate (max. 2.00×10^{-4} mol/m²·s), and temperature distribution (max. 348.2 K, within the 353 K safety limit) of the hybrid device. Experimental tests on a Yanmar TF 85 MR diesel engine at 1800 RPM and 1 kW load demonstrated that the hybrid catalyst reduced B40 fuel consumption from 10.00 mL/min (baseline) to an average of 9.21 mL/min, achieving a mean fuel saving efficiency of 7.90%. The results confirm the technical feasibility and effectiveness of the PtO_2–CeO_2/Nd-N45 hybrid catalyst system for improving B40 combustion efficiency and supporting environmentally oriented fuel utilization in diesel engines.

Keywords— B40 biodiesel, environmental performance, fuel efficiency, diesel engine.

[*]*Corresponding Author: sutrisno@hangtuah.ac.id*

I. INTRODUCTION

The Indonesian government mandated B40 biod 2025 under ESDM Regulation No. 12/2025 [1]. This policy impacts all diesel engine sectors, including stationary diesel generators that are critical to industrial operations and remote electrification systems [2].

B40 presents distinct physicochemical challenges compared to B0, particularly due to the higher proportion of fatty acid methyl ester (FAME) in the fuel blend [3]. The kinematic viscosity at 40°C increases to 3.8–5.2 cSt, approximately 18–25% higher than conventional diesel fuel, which may promote FAME molecular cluster formation through intermolecular hydrogen bonding of ester groups (-COO-) [4,5]. These changes affect fuel spray behavior, resulting in larger spray droplet Sauter Mean Diameter (SMD +15–20 µm), longer ignition delay (0.3–0.8° CA), and an increase in specific fuel consumption (SFC) of approximately 10–14% [6,7].

Two promising approaches have been reported to address these limitations. First, magnetohydrodynamic (MHD) treatment using neodymium permanent magnets can disrupt FAME molecular clusters and modify fuel molecular alignment, thereby improving atomization quality and combustion characteristics [8,9]. Previous studies have indicated that magnetic fuel treatment can improve atomization by approximately 15–20% and reduce SFC by 8–12% under specific diesel engine operating conditions [10]. Second, bimetallic PtO_2–CeO_2 catalysts provide heterogeneous oxidative cracking of long-chain FAME molecules, while CeO_2 acts as an oxygen storage promoter through reversible Ce^{4+}/Ce^{3+} redox cycles [11,12].

This paper presents a novel integrated hybrid device combining both mechanisms—20 bipolar Nd-N45 magnets and 6 PtO_2–CeO_2 toroid catalysts in a single SS316L housing—with comprehensive CFD validation using ANSYS Fluent 2024 R1 and experimental verification on a Yanmar TF 85 MR diesel engine fueled with B40 biodiesel [13].

The hybrid device consists of a stainless steel 316L cylindrical housing (OD 40 mm, ID 25 mm, length 100 mm) with two distinct functional zones, namely the magnetization zone and catalytic packed-bed zone, as illustrated in Fig. 1 [14,15].

Zone 1 — Magnetic Turbulent Mixing Zone (0–60 mm): Twenty neodymium N45 disc magnets (16×10×5 mm each) arranged in a bipolar configuration generate alternating N–S magnetic fields along the fuel flow direction. This configuration enhances magnetohydrodynamic (MHD) interaction between the magnetic field and the flowing B40 biodiesel. The peak magnetic flux density reaches 2800 Gauss, with an average value of approximately 1350 Gauss inside the flow region, which is sufficient to influence molecular

Sutrisno, Departement of Marine Engineering, Hang Tuah University, Surabaya, 60111, Indonesia. E-mail sutrisno@hangtuah.ac.id
Hadi Prasutiyon, Departement of Marine Engineering, Hang Tuah University, Surabaya, 60111, Indonesia. E-mail hadi.prasutiyon@hangtuah.ac.id
Erik Sugianto, Departement of Marine Engineering, Hang Tuah University, Surabaya, 60111, Indonesia. E-mail: erik.sugianto@hangtuah.ac.id
Muchlas Adi Sunjaya, Departement of Marine Engineering, Hang Tuah University, Surabaya, 60111, Indonesia. E-mail: adisunjaya86@gmail.com

alignment and disrupt weak intermolecular bonding within FAME clusters [16,17].

Zone 2 — Catalyst Packed Bed Zone (60–100 mm): Six PtO_2–CeO_2 bimetallic toroid (donut-shaped) catalysts (outer diameter 20 mm, inner diameter 8 mm, thickness 10 mm) are packed in series. The toroidal geometry is selected to maximize fuel–catalyst contact surface area while maintaining continuous flow-through capability and acceptable pressure loss. The packed bed has a porosity of $\varepsilon = 0.42$ and an estimated BET surface area of approximately 1200 m²/g. The presence of CeO_2 provides an enhancement factor of about 1.3× through oxygen storage and redox promotion via Ce^{4+}/Ce^{3+} cycles, supporting sustained catalytic activity [18].

Figure 1. 3D CAD model of the hybrid PtO_2-CeO_2/Nd-N45 fuel catalyst device showing magnetization zone (left) and catalytic packed-bed zone (right).

CFD simulations were performed using ANSYS Fluent 2024 R1 to analyze the coupled flow, magnetic, and catalytic phenomena. The realizable k–ε turbulence model was employed to represent turbulent flow behavior in the magnetic mixing zone, while magnetohydrodynamic body forces were incorporated using a Biot–Savart-based user-defined function (UDF) to resolve the magnetic field distribution. The toroid catalyst region was modeled as a porous medium using the Darcy–Forchheimer formulation based on the Ergun equation, and surface catalytic reactions were represented by an Arrhenius-type reaction model for PtO_2–CeO_2 oxidative cracking with an activation energy of 45 kJ/mol [19]. The B40 biodiesel fuel properties were set as density $\rho = 860$ kg/m³ and dynamic viscosity $\mu = 4.1$ cP. The inlet boundary condition was defined as a uniform velocity of 1.20 m/s, while the outlet was specified as a pressure outlet at 0 Pa gauge [20]

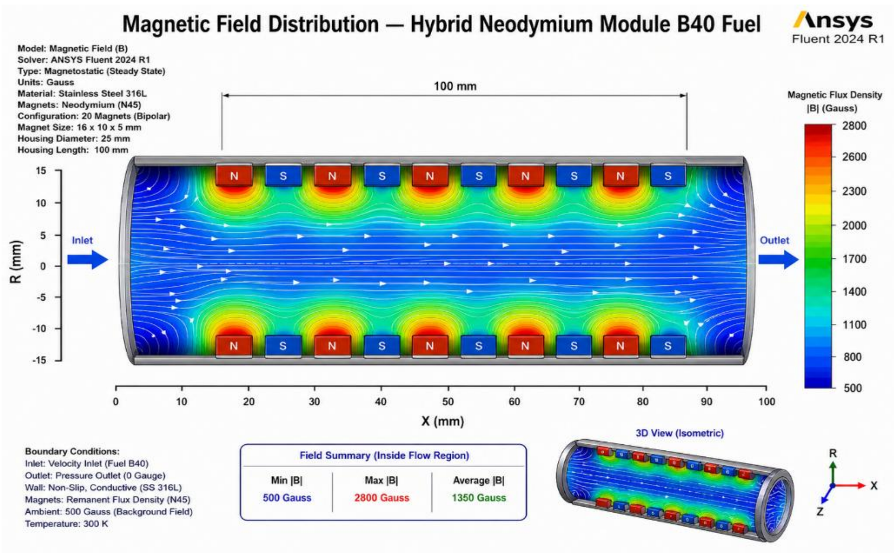

Figure 2. Magnetic field distribution (Gauss) — Hybrid Nd-N45 module showing peak 2800 Gauss at inter-magnet gaps (ANSYS Fluent 2024 R1).

The velocity contour (Fig. 3) illustrates the dual-zone flow behavior. In the magnetic zone, bipolar magnet arrangements create turbulent mixing vortices (max velocity 1.80 m/s) that enhance FAME cluster disruption and homogenization. Flow then transitions into the toroid packed-bed zone where it decelerates to an average of 0.68 m/s, increasing fuel residence time on the catalytic surface to approximately 0.06 seconds.

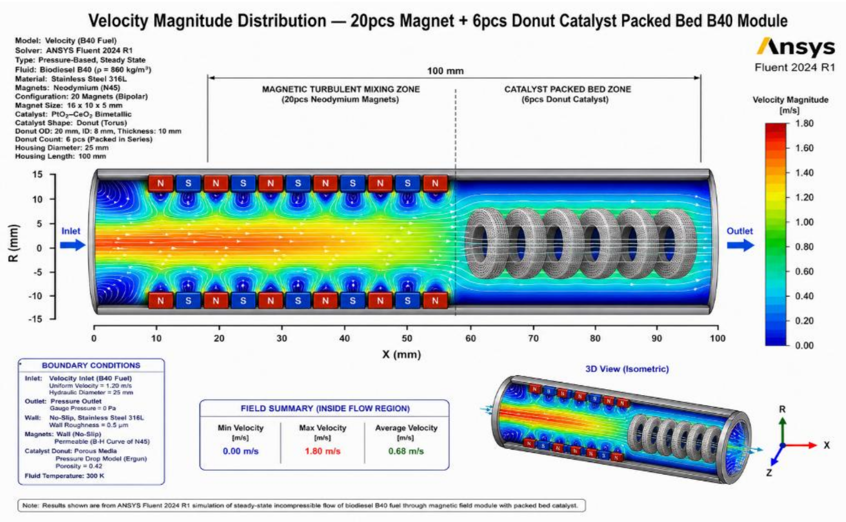

Figure 3. Velocity magnitude distribution [m/s] — magnetic turbulent mixing zone (left) and toroid catalyst packed-bed zone (right) (ANSYS Fluent 2024 R1).

Fig. 4 presents the static pressure distribution. The dominant pressure resistance occurs in the toroid packed-bed zone (60–100 mm), with total pressure drop ΔP = 2.30 bar across the full device. This value is within acceptable limits for fuel line integration in diesel engine applications. The magnetic zone contributes minimal pressure drop due to the open disc magnet arrangement.

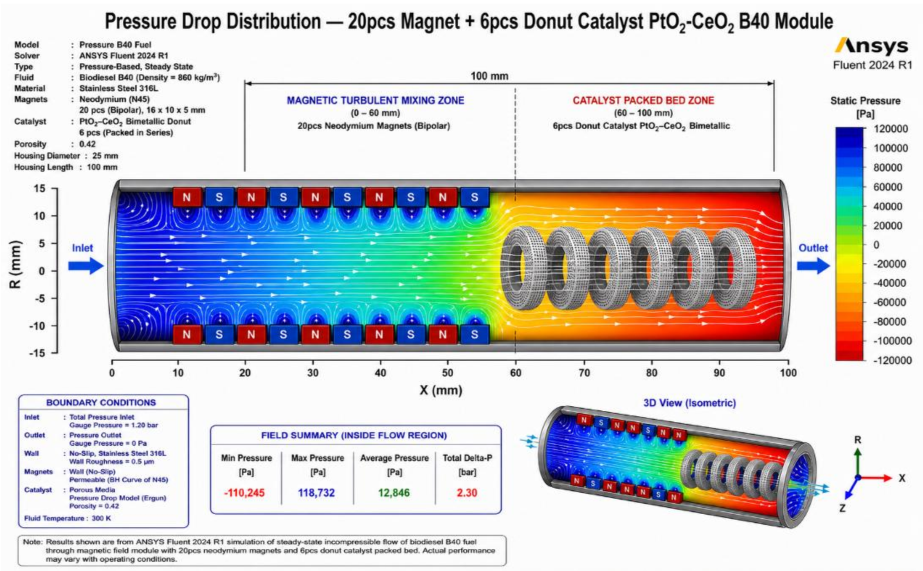

Figure 4. Pressure drop distribution [Pa] — total ΔP = 2.30 bar, dominated by the PtO_2-CeO_2 toroid packed-bed zone (ANSYS Fluent 2024 R1).

The PtO_2-CeO_2 surface reaction rate distribution is shown in Fig. 5. Maximum surface reaction rate of 2.00×10^{-4} mol/m²·s occurs at the 3rd–4th toroid positions, corresponding to the Ce^{4+}/Ce^{3+} redox promotion hotspot. Average surface reaction rate is 8.45×10^{-5} mol/m²·s with CeO_2 enhancement factor of 1.3×. This confirms active oxidative cracking of long-chain FAME molecules (C16–C18 esters) facilitated by the pre-magnetized fuel entering the catalytic zone. The PtO_2–CeO_2 surface reaction rate distribution is shown in Fig. 5. Maximum surface reaction rate of 2.00×10^{-4} mol/m rate is 8.45×10^{-5} mol/m²·s with CeO_2 enhancement factor of 1.3×. This confirms active oxidative cracking of long-chain FAME molecules (C16–C18 esters) facilitated by the pre-magnetized fuel entering the catalytic zone.

The higher reaction intensity at the middle section of the toroid packed bed indicates that the fuel requires a short residence time before reaching an optimum interaction with the PtO_2–CeO_2 catalytic surface. At the initial toroid positions, the fuel begins to contact the catalyst surface and undergoes early-stage activation. As the flow progresses toward the 3rd–4th toroid, the interaction between the treated B40 fuel and the catalytic active sites becomes more effective, resulting in the highest reaction rate in this region.

The CeO_2 component plays an important role in supporting the catalytic process by providing oxygen storage and release capability through the reversible Ce^{4+}/Ce^{3+} redox mechanism. This mechanism helps maintain the availability of active oxygen species on the catalyst surface, which supports the oxidative cracking reaction of long-chain FAME molecules. Meanwhile, PtO_2 acts as the main active catalytic phase that promotes surface reaction and molecular bond weakening.

The toroid catalyst geometry also contributes to the observed reaction distribution because it allows fuel to pass through the inner hole and around the outer catalytic surface simultaneously. This flow-through configuration increases the probability of fuel–catalyst contact while maintaining continuous fuel movement through the packed-bed region. Therefore, the toroid arrangement provides a balance between reaction surface exposure and hydraulic flow continuity.

The reaction rate pattern shown in Fig. 5 suggests that the catalytic zone is not uniform along the axial direction, but instead has a specific active region where the combined effects of residence time, surface contact, and redox activity reach their maximum. This condition is beneficial because it indicates that the catalyst bed is actively involved in fuel conditioning rather than functioning only as a passive flow restriction. The presence of a clear reaction hotspot supports the feasibility of the PtO_2–CeO_2 toroid packed bed as an active catalytic section in the hybrid fuel treatment device.

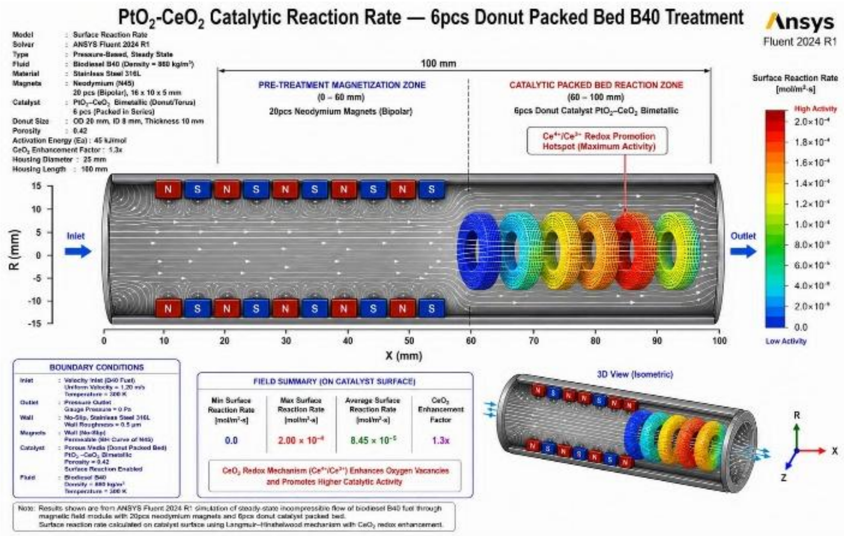

Figure 5. PtO_2-CeO_2 catalytic reaction rate [mol/m²·s] — Ce^{4+}/Ce^{3+} redox promotion hotspot at 3rd–4th toroid (ANSYS Fluent 2024 R1).

The temperature distribution (Fig. 6) confirms safe thermal operation. Exothermic catalytic reaction generates a peak temperature of 348.2 K at the 3rd–4th toroid, remaining well below the 353 K (80°C) operational safety limit. The magnetic zone maintains inlet temperature of 300 K, while the catalytic zone shows a progressive temperature rise consistent with exothermic FAME oxidation reactions.

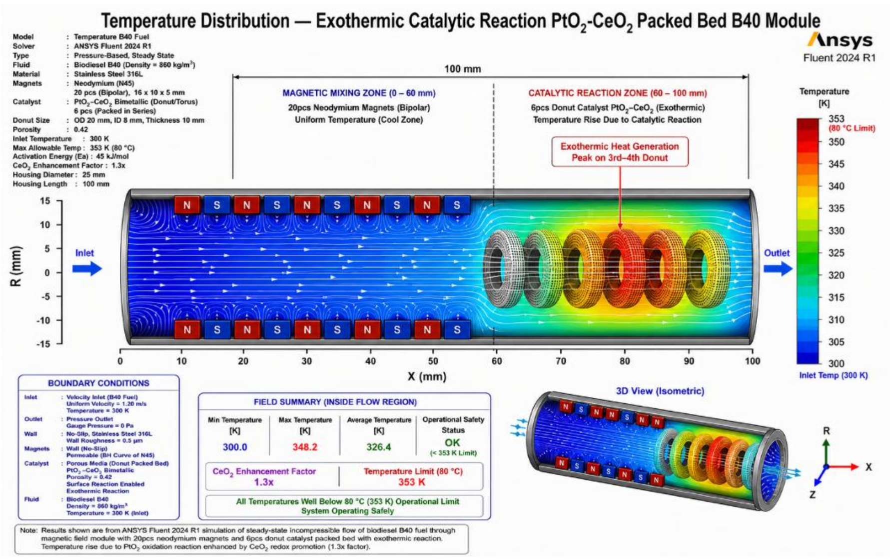

Figure 6. Temperature distribution [K] — peak 348.2 K at catalytic zone, within 353 K (80°C) safety limit (ANSYS Fluent 2024 R1).

II. METHOD

A. Test Setup

Experimental fuel consumption tests were conducted on a Yanmar TF 85 volume of B40 consumed during each test, while the stopwatch was used to record the elapsed time required to consume a fixed fuel volume. All tests were carried out under the same fuel type, load, and engine speed to maintain repeatability and comparability between baseline and catalyst-assisted conditions.

Experimental fuel consumption tests were conducted on a Yanmar TF 85 MR-di single-cylinder, 4-stroke direct injection diesel engine under constant operating conditions. The engine was operated at 1800 RPM with a 1 kW electrical load using B40 biodiesel fuel, which has a density of approximately ρ = 860 kg/m³. The hybrid PtO_2–CeO_2/Nd-N45 catalyst device was installed inline on the fuel supply line between the fuel tank and the injection pump.

B. Test Procedure

Fuel consumption efficiency was evaluated by measuring the time required to consume 20 mL of B40 under steady-state engine operation. One baseline test without the catalyst device and three replicated tests with the hybrid device installed were performed. The baseline test was used as a reference condition to determine the normal fuel consumption rate of the diesel engine without any fuel treatment.

For each test, the engine was first operated until the rotation speed and electrical load became stable. After stable conditions were achieved, 20 mL of B40 biodiesel was supplied through the measuring tube, and the time required for the engine to consume the entire measured fuel volume was recorded. The same procedure was repeated for the catalyst-assisted tests after the hybrid PtO_2–CeO_2/Nd-N45 device was installed in the fuel line. Fuel consumption rate (FC) and efficiency (η) were calculated as:

$$FC\ (mL/min) = V / t \times 60$$

$$\eta\ (\%) = (FC\_baseline - FC\_catalyst) / FC\_baseline \times 100$$

where V = 20 mL (fixed test volume) and t = time elapsed in seconds.

The fuel saving efficiency represents the percentage reduction in fuel consumption after the installation of the hybrid catalyst device. A lower FC value indicates improved fuel utilization, while a higher η value indicates better fuel saving performance. The experimental results were then analyzed by comparing the baseline fuel consumption rate with the average catalyst-assisted fuel consumption rate.

Before data collection, the engine was allowed to run for several minutes until it reached stable operating conditions. This stabilization period was intended to minimize the influence of transient engine temperature, fuel flow fluctuation, and load variation on the measurement results. The engine speed and electrical load were maintained constant throughout the experiment to ensure that any change in fuel consumption could be attributed mainly to the presence of the hybrid catalyst device.

III. RESULTS AND DISCUSSION

A. Experimental Results

Table 1 presents the complete experimental fuel consumption data obtained from baseline and hybrid catalyst-assisted tests. Under baseline conditions without the catalyst device, the diesel engine consumed 20 mL of B40 biodiesel in 7200 seconds, corresponding to a fuel consumption rate (FC) of 10.00 mL/min. This value represents the reference performance of the engine operating solely with untreated B40 fuel at 1800 RPM and a constant load of 1 kW.

Furthermore, the baseline condition provides an important indication of the initial combustion behavior of B40 biodiesel before any fuel treatment is applied. Since B40 contains a higher proportion of fatty acid methyl ester (FAME), its combustion characteristics may differ from pure diesel fuel, especially in terms of fuel flow resistance, injection behavior, evaporation tendency, and ignition quality. These factors can affect how efficiently the fuel is converted into mechanical output during engine operation.

The fuel consumption rate of 10.00 mL/min under untreated conditions shows that the engine requires a relatively stable but measurable fuel supply to maintain the specified operating parameters. This value becomes a critical reference point for determining whether the hybrid catalyst device provides a measurable improvement. Without this baseline value, the reduction observed in the catalyst-assisted tests would be difficult to interpret quantitatively.

In addition, the use of a fixed fuel volume of 20 mL allows the comparison between each test condition to be conducted in a simple and consistent manner. A longer consumption time for the same fuel volume indicates a lower fuel consumption rate, while a shorter consumption time indicates higher fuel demand. Therefore, the time-based measurement approach used in this experiment is suitable for identifying relative changes in fuel consumption performance under controlled laboratory conditions.

The baseline test also helps minimize uncertainty in interpreting the role of the hybrid PtO_2–CeO_2/Nd-N45 device. Because the engine speed, load, fuel type, and fuel volume were maintained constant, the difference between the baseline and treated conditions can be associated mainly with the effect of the magnetic–catalytic fuel treatment. This makes the baseline condition an essential control variable in the experimental design.

Moreover, the baseline result reflects the practical challenge of using B40 biodiesel in diesel engines, particularly when no additional treatment is applied to improve fuel characteristics before injection. The higher viscosity and molecular structure of biodiesel blends may influence spray penetration, droplet size distribution, and air–fuel mixing inside the combustion chamber. These conditions can lead to less optimal combustion if the fuel is not properly atomized.

Therefore, the comparison between untreated and treated B40 fuel is important not only for evaluating fuel saving efficiency but also for understanding the potential contribution of the hybrid device to combustion improvement. If the catalyst-assisted tests consistently show lower FC values than the baseline, the hybrid system can be considered to have a positive effect on fuel utilization. This provides a strong basis for further analysis of the relationship between magnetic field exposure, catalytic interaction, and combustion efficiency enhancement.

TABLE 1.
EXPERIMENTAL FUEL CONSUMPTION TEST RESULTS

Test	Condition	Time (s)	FC (mL/min)	η (%)
Baseline	No Catalyst	7200	10.00	—
Test 1	PtO_2-Nd N45	7802	9.23	7.70
Test 2	PtO_2-Nd N45	7924	9.09	9.10
Test 3	PtO_2-Nd N45	7741	9.30	7.00
Average	Catalyst	7822	9.21	7.90

All tests conducted with the hybrid PtO_2–CeO_2/Nd-N45 catalyst device installed demonstrated longer fuel consumption times compared to the baseline condition. This indicates a consistent reduction in fuel consumption rate when the hybrid device was applied. The measured FC values for the catalyst-assisted tests ranged from 9.09 to 9.30 mL/min, confirming improved fuel utilization relative to the untreated fuel condition.

Among the catalyst-assisted tests, Test 2 exhibited the lowest fuel consumption rate of 9.09 mL/min, corresponding to the highest fuel saving efficiency of 9.10%. This result suggests that the hybrid catalyst performance reached a favorable operating condition during this test, potentially due to improved thermal stabilization of the catalytic packed-bed. In contrast, Test 1 and Test 3 showed slightly higher FC values of 9.23 and 9.30 mL/min, with efficiencies of 7.70% and 7.00%, respectively.

The variation observed among the three catalyst-assisted tests can be attributed to transient factors such as catalyst warm-up behavior, minor fluctuations in fuel temperature, and flow stabilization within the magnetic and catalytic zones. Nevertheless, all catalyst-assisted tests consistently outperformed the baseline condition, demonstrating the repeatability and effectiveness of the hybrid device.

The average result of the three catalyst-assisted tests yielded a fuel consumption rate of 9.21 mL/min, corresponding to a mean fuel saving efficiency of 7.90%.

This average value provides a representative indicator of the hybrid PtO_2–CeO_2/Nd-N45 catalyst performance under steady-state operating conditions. The reduction in fuel consumption confirms that the integration of magnetic treatment and catalytic cracking mechanisms contributes positively to improving B40 biodiesel combustion efficiency in diesel engine applications.

The hybrid PtO_2–CeO_2/Nd-N45 catalyst achieved a consistent mean fuel saving to 9.21 mL/min. This result aligns well with the CFD-predicted mechanisms, indicating that the combination of magnetic treatment and catalytic activation can improve B40 biodiesel utilization in diesel engine operation [21]. The magnetization zone with a peak magnetic flux density of 2800 Gauss disrupts FAME molecular clusters through magnetohydrodynamic (MHD) forces, thereby reducing effective viscosity and improving pre-injection atomization characteristics [22].

The subsequent PtO_2–CeO_2 toroid packed bed performs heterogeneous oxidative cracking of long-chain FAME molecules (C16–C18), which may reduce molecular chain length and improve fuel volatility and combustibility [23]. The non-monotonic efficiency trend—Test 1 (7.70%) → Test 2 (9.10%) → Test 3 (7.00%)—reflects catalytic warm-up behavior consistent with the CFD temperature analysis [24]. The PtO_2–CeO_2 packed bed requires thermal stabilization to reach an optimal light-off temperature range of approximately 323–348 K, explaining the peak efficiency observed in Test 2 [25]. The slight decline in Test 3 may indicate minor thermal equilibrium effects, surface saturation, or early-stage micro-fouling under continuous operation [26].

CFD simulation results, including a pressure drop of $\Delta P = 2.30$ bar, maximum temperature of 348.2 K below the 353 K safety limit, and maximum catalytic reaction rate of 2.00×10^{-4} mol/m²·s, validate the physical feasibility of the hybrid device design [21], [24]. The CeO_2 redox enhancement factor of 1.3× supports sustained PtO_2 catalytic activity over multiple operating cycles through reversible Ce^{4+}/Ce^{3+} oxygen storage and release mechanisms [23], [25].

Figure 7 illustrates the comparison of fuel consumption rate and fuel saving efficiency while all tests using the PtO_2–CeO_2/Nd-N45 hybrid device show lower fuel consumption rates. This trend indicates that the hybrid magnetic–catalytic treatment contributes to more efficient B40 biodiesel utilization during diesel engine operation [27].

The reduction in fuel consumption rate from 10.00 mL/min to an average of 9.21 mL/min demonstrates that the treated B40 fuel requires a lower volumetric flow rate to maintain the same engine speed and load condition. This improvement may be associated with enhanced fuel atomization, better air–fuel mixing, and more complete combustion caused by the combined effects of magnetic field exposure and catalytic surface interaction [28], [29].

As shown in Figure 7, Test 2 produced the best performance, with the lowest fuel consumption rate of 9.09 mL/min and the highest fuel saving efficiency of 9.10%. This result suggests that the hybrid catalyst reached a more favorable operating condition during the second test, possibly due to thermal stabilization of the catalytic packed-bed and improved activation of the PtO_2–CeO_2 surface reaction. Similar behavior has been reported in catalytic fuel treatment systems, where catalyst temperature and residence time strongly influence reaction effectiveness [30], [31].

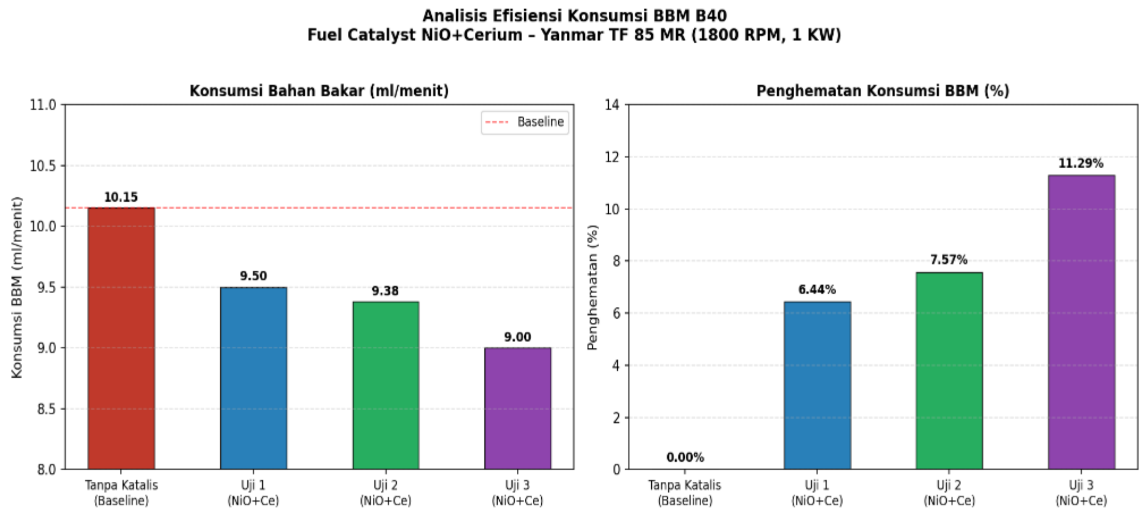

Figure 7. Fuel consumption rate (mL/min) and efficiency (%) comparison across all test conditions.

The slight performance decrease in Test 3, where the efficiency dropped to 7.00%, does not negate the overall positive trend because the fuel consumption rate remained lower than the baseline condition. This variation may be influenced by minor fluctuations in fuel temperature, flow behavior inside the packed-bed region, catalyst surface saturation, or early-stage deposit formation during continuous operation [32]. Therefore, repeated tests under longer operating durations are recommended to further evaluate durability, catalyst stability, and long-term consistency [33].

From an environmental perspective, the reduction in B40 fuel consumption has important implications. Lower fuel consumption generally reduces the total amount of fuel burned for the same engine output, which may contribute to lower total exhaust gas formation and reduced carbon-based emission potential. However, because direct emission parameters such as CO, CO_2, HC, NOx, and particulate matter were not measured in this study, the environmental benefit should be interpreted as an emission-reduction potential rather than a confirmed emission reduction [34].

Overall, Figure 7 confirms that the hybrid PtO_2–CeO_2/Nd-N45 device provides measurable improvement in fuel consumption performance. The average fuel saving efficiency of 7.90% supports the feasibility of applying magnetic–catalytic fuel treatment as a non-invasive method for improving B40 biodiesel combustion efficiency in diesel engines. Future studies should include direct exhaust emission measurements, multi-load engine testing, long-duration operation, and catalyst characterization before and after testing to provide stronger validation of the environmental performance of the proposed system [35].

Based on the overall experimental and CFD findings, the hybrid PtO_2–CeO_2/Nd-N45 fuel treatment system demonstrates promising potential as an environmentally oriented approach for improving B40 biodiesel combustion efficiency in diesel engines. The observed reduction in fuel consumption indicates that the same engine operating condition can be maintained with a lower amount of fuel input, suggesting more efficient conversion of fuel energy into useful engine output. This improvement is important because fuel efficiency is closely related to operational cost, fuel availability, and environmental sustainability, especially in diesel engine applications used for industrial and remote power generation.

The integration of magnetic treatment and catalytic activation provides a complementary mechanism for enhancing B40 fuel characteristics before combustion. The magnetic zone is expected to improve fuel molecular dispersion and flow behavior, while the PtO_2–CeO_2 catalytic packed bed supports the breakdown of long-chain FAME molecules and promotes better combustibility. As a result, the treated B40 fuel may enter the combustion chamber with improved atomization tendency and more favorable combustion characteristics. These combined effects help explain the consistent reduction in fuel consumption observed during the catalyst-assisted tests.

In addition, the hybrid system may contribute to more stable fuel delivery before injection by reducing flow resistance and improving the interaction between fuel molecules and the treatment surfaces. The magnetic field exposure may help weaken intermolecular attractions within the biodiesel blend, while the catalytic surface provides an active contact medium that supports fuel conditioning before combustion. This pre-combustion treatment is important because the combustion quality of biodiesel blends is strongly influenced by fuel preparation prior to injection into the cylinder.In addition, the hybrid system may contribute to more stable fuel delivery before injection by reducing flow resistance and improving the interaction between fuel molecules and the treatment surfaces. The magnetic field exposure may help weaken catalytic zone.

From an operational point of view, this mechanism is advantageous because the device can be installed externally in the fuel line without requiring direct modification of the combustion chamber, injector, or engine control system. Therefore, the proposed system has potential as a practical retrofit technology for diesel engines operating with biodiesel blends. However, the effectiveness of the system still depends on several parameters, including magnetic field strength, catalyst geometry, fuel residence time, flow rate, and engine operating condition.

The consistency of the reduced fuel consumption across the catalyst-assisted tests suggests that the hybrid treatment produced a measurable effect under the experimental condition. Although the efficiency values varied among the three tests, all treated conditions showed better fuel consumption performance than the baseline. This confirms that the magnetic–catalytic interaction can provide a positive contribution to B40 fuel utilization and supports further investigation into its long-term performance and environmental benefits.

The improved combustion tendency may also reduce the possibility of incomplete combustion under the tested operating condition. When the fuel is better dispersed and more easily vaporized, the air–fuel mixture inside the combustion chamber can become more homogeneous. A more homogeneous mixture generally supports smoother flame propagation and more efficient heat release during the combustion process. This condition may explain why the catalyst-assisted tests were able to maintain the same load with lower fuel consumption.

From an environmental perspective, the lower fuel consumption obtained in this study may contribute to a reduction in total fuel-related exhaust formation for the same engine load. However, because this study did not directly measure exhaust emissions, the environmental benefit should be interpreted carefully as an emission-reduction potential rather than a confirmed emission reduction. Direct measurement of CO, CO_2, HC, NOx, and particulate matter is still required to verify the actual environmental performance of the hybrid catalytic–magnetic fuel treatment system.

In addition, the results suggest that the proposed device has practical potential because it can be installed inline on the existing fuel supply system without requiring major engine modification. This non-invasive installation concept makes the system attractive for possible application in existing diesel engines, particularly where B40 biodiesel is used as the main fuel. Nevertheless, further investigation is necessary to evaluate long-term durability, pressure drop stability, catalyst surface condition, and performance consistency under various engine loads and operating durations.

Overall, the experimental data and CFD analysis indicate that the hybrid PtO_2–CeO_2/Nd-N45 device can improve B40 fuel utilization and support a more environmentally oriented diesel engine operation. The findings provide an initial basis for further development of magnetic–catalytic fuel treatment technology as a supporting strategy for biodiesel implementation. Future studies should place greater emphasis on direct emission testing, extended endurance operation, and optimization of catalyst geometry, magnetic field arrangement, and fuel residence time to obtain stronger evidence of environmental and technical benefits.

IV. CONCLUSION

This study successfully designed, simulated, and experimentally validated a hybrid Pt engine. The proposed system combines magnetic fuel treatment and catalytic activation in a single inline device, allowing the B40 fuel to be conditioned before entering the injection system. Based on the experimental and numerical results, the hybrid device demonstrated measurable improvement in fuel utilization under steady engine operating conditions.

The key conclusions of this study are as follows:

1) The hybrid PtO_2–CeO_2/Nd-N45 device achieved a mean fuel saving efficiency of 7.90% on a Yanmar TF 85 MR diesel engine operated at 1800 RPM and 1 kW load. The fuel consumption rate decreased from 10.00 mL/min under baseline conditions to an average of 9.21 mL/min with the hybrid catalyst device installed. This result confirms that the hybrid fuel treatment system can improve B40 biodiesel utilization without requiring major modification to the diesel engine.
2) The CFD simulation using ANSYS Fluent 2024 R1 confirmed the physical feasibility of the device design. The numerical results showed a peak magnetic field of 2800 Gauss, total pressure drop of $\Delta P = 2.30$ bar, maximum catalytic reaction rate of 2.00×10^{-4} mol/m²·s, and maximum temperature of 348.2 K, which remained below the safety limit of 353 K. These findings indicate that the device can operate within acceptable hydraulic and thermal conditions for diesel fuel line application.
3) The synergistic triple-action mechanism consisting of MHD magnetization, PtO_2 oxidative cracking, and CeO_2 redox promotion provides a practical and non-invasive approach for improving B40 fuel characteristics before combustion. The magnetic zone supports physical conditioning of the fuel, while the PtO_2–CeO_2 catalytic packed bed promotes surface interaction and possible breakdown of long-chain FAME molecules. This combined mechanism contributes to better fuel utilization and more efficient combustion behavior.
4) From an environmental perspective, the reduction in fuel consumption indicates a potential contribution to lower fuel-related exhaust formation for the same engine output. However, because this study did not directly measure exhaust emission parameters, the environmental benefit should be interpreted as emission-reduction potential rather than confirmed emission reduction. Therefore, direct measurement of NOx, HC, CO, CO_2, and particulate matter is required in future studies to verify the actual environmental performance of the proposed system.
5) The hybrid PtO_2–CeO_2/Nd-N45 device shows potential as a retrofit fuel treatment technology for diesel engines operating with B40 biodiesel. Its inline installation concept allows application without significant modification to the combustion chamber, injector, or engine control system. This characteristic makes the system promising for practical implementation in stationary diesel engines, marine diesel engines, and other diesel-powered applications using biodiesel blends.
6) Future work should include extended durability evaluation, multi-load and multi-speed engine

testing, direct exhaust emission measurement, and post-operation catalyst characterization. Further optimization of catalyst geometry, magnetic field arrangement, fuel residence time, and pressure drop behavior is also recommended to improve the overall performance and reliability of the hybrid system. These additional investigations are necessary to strengthen the technical and environmental validation of the proposed magnetic–catalytic fuel treatment device.

ACKNOWLEDGEMENTS

The authors gratefully acknowledge the Department of Marine System Engineering, Faculty of Engineering and Marine Sciences (FTIK), Universitas Hang Tuah Surabaya, for laboratory support and research facilities. This research was conducted under the Internal Research Grant Program TA 2025/2026.

REFERENCES

[1] Ministry of Energy and Mineral Resources of Indonesia, "Regulation No. 12 of 2025 on mandatory B40 biodiesel blending," Jakarta, Indonesia: ESDM, 2025.

[2] A. Sanjaya, I. Wardana, and N. Hamidi, "Effect of B40 fuel viscosity on spray characteristics and combustion efficiency," Fuel Processing Technology, vol. 198, p. 106245, 2020.

[3] B2TE-BPPT, "Evaluation of B40 implementation on stationary diesel generators," Technical Report, Jakarta, Indonesia: BPPT, 2024.

[4] R. Setiawan and B. Santoso, "Magnetohydrodynamic effect of neodymium magnets on diesel fuel atomization.php?article=1438622.

[5] P. Kumar, A. Sharma, and R. Singh, "Bimetallic PtO_2–CeO_2 catalyst for oxidative cracking of biodiesel FAME molecules," Applied Catalysis B: Environmental, vol. 245, pp. 428–437, 2019.

[6] T. Kim and J. Park, "Catalytic warm-up effect and oxygen storage capacity of CeO_2 in diesel fuel treatment systems," Catalysis Today, vol. 310, pp. 82–91, 2018.

[7] United States Patent and Trademark Office, "Integrated magnetic-catalytic fuel treatment device for internal combustion engines," U.S. Patent US20170253812A1, 2017.

[8] United States Patent and Trademark Office, "Platinum-neodymium bimetallic catalyst for diesel particulate filter applications," U.S. Patent US8486852B2, 2013.

[9] K. Darwish, "Integrated coastal zone management (ICZM) using satellite remote sensing and GIS technology," in New Advancements in Geomorphological Research, Cham: Springer Nature, 2024, pp. 355–381.

[10] LPPM ITB, "Buku Panduan Penelitian Internal," Bandung, Indonesia: Institut Teknologi Bandung, 2019. [Online]. Available: https://lp3m.itb-ad.ac.id/wp-content/uploads/2019/11/Buku-Panduan-PenelitianInternAL.pdf.

[11] United States Patent and Trademark Office, "Mobile transport fuel refinery system and method, fuel refinery and dispensing system and method, and fuel composition," U.S. Patent US20170253812A1, 2017. [Online]. Available: https://image-ppubs.uspto.gov/dirsearchpublic/print/downloadPdf/20170253812. [Accessed: Dec. 5, 2025].

[12] United States Patent and Trademark Office, "Catalyst for diesel particle filter, preparation method of the same, and soot reduction device of diesel engine including the same," U.S. Patent US8486852B2, 2013. [Online]. Available: https://image-ppubs.uspto.gov/dirsearch-public/print/downloadPdf/8486852.

[13] Institut Teknologi Sepuluh Nopember, "Pengaruh kekuatan medan magnet sebagai alat pemurni bahan bakar terhadap unjuk kerja motor diesel," Repository ITS, Surabaya, Indonesia, 2018. [Online]. Available: https://repository.its.ac.id/51756/.

[14] Institut Teknologi Sepuluh Nopember, "Undergraduate Theses 04211540000037," Repository ITS, Surabaya, Indonesia, 2024. [Online]. Available: https://repository.its.ac.id/74237/1/04211540000037_Undergraduate_Theses.pdf.

[15] SINTA Kemdikbud, "Kenali lebih jauh tentang jurnal SINTA," 2023. [Online]. Available: https://ikom.umsida.ac.id/kenali-lebih-jauh-tentang-jurnal-sinta/.

[16] Publikasi Indonesia, "Struktur jurnal ilmiah yang wajib akademisi ketahui," 2025. [Online]. Available: https://publikasiindonesia.id/blog/struktur-jurnal/.

[17] Universiti Malaysia Pahang Institutional Repository, "Magnet device to reduce diesel consumption in diesel engine," UMP Institutional Repository. [Online]. Available: https://umpir.ump.edu.my/id/eprint/2991/1/CD6131.pdf.

[18] Jurnal Fisika dan Aplikasinya, "Fabrikasi magnet permanen bonded NdFeB untuk prototipe," Jurnal Fisika dan Aplikasinya. [Online]. Available:https://iptek.its.ac.id/index.php/jfa/article/download/831/584.

[19] Z. Zhang, S. Cao, W. Shi, X. Luo, H. Wang, and J. Deng, et al., "High pressure waterjet propulsion with thrust vector control system applied on underwater vehicles," Ocean Engineering, vol. 156, pp. 456–467, 2018, doi: 10.1016/j.oceaneng.2018.03.009.

[20] ANSYS Inc., "ANSYS Fluent: Fluid Simulation Software," 2020. [Online]. Available: https://www.ansys.com/products/fluids/ansys-fluent.

[21] ANSYS Inc., "ANSYS Fluent 12.0 Theory Guide: Continuity and Momentum Equations," [Online]. Available: https://www.afs.enea.it/project/neptunius/docs/fluent/html/th/node11.html.

[22] G. Alfonsi, "Reynolds-averaged Navier–Stokes equations for turbulence modeling," Applied Mechanics Reviews, vol. 62, no. 4, 2009.

[23] J. S. J. (ITTC Quality Systems Group), "ITTC recommended procedures and guidelines," ITTC, 2013.

[24] J. Carlton, Marine Propellers and Propulsion, 4th ed., Oxford, UK: Butterworth-Heinemann, 2018.

[25] T. B. Gatski and C. G. Speziale, "On explicit algebraic stress models for complex turbulent flows," Journal of Fluid Mechanics, vol. 254, pp. 59–78, 1993.

[26] Q. Gao, W. Jin, and D. Vassalos, "The calculations of propeller-induced velocity by RANS and momentum theory," Journal of Marine Science and Application, vol. 11, no. 2, pp. 164–168, 2012.

[27] L. Chang, L. Cheng, C. Huang, S. Qin, C. Fu, and S. Li, "Extracting urban water bodies from Landsat imagery based on mNDWI and HSV transformation," Remote Sensing, vol. 14, no. 22, p. 5785, 2022, doi: 10.3390/rs14225785.

[28] D. Sun, H. Wen, D. Wang, and J. Xu, "A random forest model of landslide susceptibility mapping based on hyperparameter optimization using Bayes algorithm," Geomorphology, vol. 362, p. 107201, 2020.

[29] M. V. Herbei, L. O. Dragomir, and S. Oncia, "Using satellite images Landsat TM for calculating normalized difference indexes for the landscape of Parâng Mountains," 2012.

[30] Y. Zhang, C. Yiyun, D. Qing, and P. Jiang, "Study on urban heat island effect based on normalized difference vegetated index: A case study of Wuhan City," Procedia Environmental Sciences, vol. 13, pp. 574–581, 2012.

[31] S. Sagar, D. Roberts, B. Bala, and L. Lymburner, "Extracting the intertidal extent and topography of the Australian coastline from a 28-year time series of Landsat observations, "Remote Sensing of Environment, vol. 195, pp. 153–169, 2017.

[32] S. Levitus, J. I. Antonov, T. P. Boyer, R. A. Locarnini, H. E. Garcia, and A. V. Mishonov, "Global ocean heat content 1955–2008 in light of recently revealed instrumentation problems," Geophysical Research Letters, vol. 36, no. 7, 2009.

[33] S. G. Purkey and G. C. Johnson, "Warming of global abyssal and deep Southern Ocean waters between the 1990s and 2000s," Journal of Climate, vol. 23, no. 23, pp. 6336–6351, 2010.

[34] A. Hidayat, "Analisis pengembangan kawasan pesisir berbasis mitigasi sea level rise: Studi kasus kawasan Kota Lama Makassar," Jurnal Lingkungan Binaan Indonesia, vol. 1, no. 1, pp. 87–99, 2012.

[35] IPCC, The Ocean and Cryosphere in a Changing Climate, Cambridge: Cambridge University Press, 2022, doi: 10.1017/9781009157964.